Selective Breakdown of Phonon Quasiparticles across Superionic Transition in $CuCrSe_2$

J. L. Niedziela,[1,2*†‡] Dipanshu Bansal,[1,2*†] Andrew F. May,[1] Jingxuan Ding,[2] Tyson Lanigan-Atkins,[2]

Georg Ehlers,[3] Douglas L. Abernathy,[3] Ayman Said,[4] & Olivier Delaire [1,2,5*]

[1]*Materials Science and Technology Division, Oak Ridge National Laboratory,*

Oak Ridge, Tennessee 37831, USA

[2]*Department of Mechanical Engineering and Materials Science, Duke University,*

Durham, North Carolina 27708, USA

[3]*Quantum Condensed Matter Division, Oak Ridge National Laboratory,*

Oak Ridge, Tennessee 37831, USA

[4]*Advanced Photon Source, Argonne National Laboratory,*

Lemont, Illinois 60439, USA

[5]*Department of Physics, Duke University,*

Durham, North Carolina 27708, USA

[*]*To whom correspondence should be addressed; E-mail:*

niedzielajl@ornl.gov, dipanshu.bansal@duke.edu, olivier.delaire@duke.edu

[†]*These authors contributed equally to this work.*

[‡]*Now at Nuclear Security and Isotope Technology Division, Oak Ridge National Laboratory*

Superionic crystals exhibit ionic mobilities comparable to liquids while maintaining a periodic crystalline lattice, thus representing an unusual intermediate between two states of matter. The atomic dynamics leading to large ionic mobility have long been debated. A central question is whether phonon quasiparticles – which conduct heat in regular solids – survive in the superionic state, where a large fraction of the system exhibits liquid-like behavior. Here, we use energy and momentum-resolved scattering studies combined with first principles calculations to achieve breakthrough insights into the lattice dynamical behavior in a superionic conductor, fully elucidating both the quasiparticle spectrum and the diffusive dynamics. We demonstrate that weak bonding and large anharmonicity of the Cu sublattice are already present in the normal state, resulting in low thermal conductivity. In the superionic state, specific phonon quasiparticles dominated by the Cu ions break down as a result of anharmonicity and disorder in the Cu sublattice, but the long-wavelength acoustic phonons remain largely intact and capable of heat conduction. These results settle long-standing controversies, and demonstrate that anharmonic phonon dynamics is common to the origin of low thermal conductivity and superionicity in this class of materials.

Differences in atomic dynamics underpin the fundamental distinction between solids and liquids [1,2]. Atoms flow in a liquid, following stochastic diffusive dynamics, while remaining affixed to well-defined lattice sites in a crystalline solid, undergoing collective oscillatory excitations in the form of phonon quasiparticles [1,2]. Superionic crystals are rare materials exhibiting crystalline order, yet support long-ranged ionic diffusion with diffusivities matching those found in liquid salts [1,3]. Despite extensive studies, the atomic dynamics in such systems remain poorly understood, and

the suitability of phonon-like descriptions has remained uncertain. These systems have attracted steady interest [1,3–5], which recently spiked with promising applications in solid-state electrolytes for safer rechargeable batteries [6–8] and in efficient thermoelectric materials [9–12]. In thermoelectric conversion of thermal gradients into useful electrical energy, the figure of merit, $zT = S^2\sigma T/\kappa$, inversely correlates thermal conductivity (κ) with electrical conductivity (σ) [13–15]. As κ in a semiconductor is dominated by the lattice component, $\kappa_{\rm lat}$, sustained efforts seek to design materials that suppress phonon propagation [16–26]. The "phonon-liquid electron-crystal" model (PLEC)[9], building on the prominent "phonon-glass electron-crystal" model[27], posits that thermal conductivity is strongly reduced in a solid through the breakdown of acoustic phonon transport in a host lattice with a liquid-like component, based on the notion that liquids do not propagate shear waves[9]. Superionic compounds could materialize the PLEC concept, achieving ultralow thermal conductivity while preserving an electronically conductive framework, and thus represent an exciting emergent class of thermoelectrics [9,11,26,28–32]. More fundamentally, the relation between phonon scattering and superionic conduction remains unclear and controversial in many superionic systems. The behavior of long-wavelength, low-energy phonon modes is a central question [9,11,26,28,29,32]. While thermal conductivity reduction through breakdown, or 'melting' of transverse acoustic (TA) modes has been proposed[9,32], it has also been argued that rattler modes with low-energy optical branches could be the main source of thermal transport suppression.[22,26,29,33,34]

$M\mathrm{Cr}X_2$ superionic conductors (M = (Li, Na, Cu, Ag), X = (Se, S)) all display very low lattice thermal conductivity and superionic liquid-like diffusivities of M ions at high temperature [11,28,30–32,35,36], and are attractive for both solid-state electrolyte and thermoelectric applications

[11,30,31,37]. The well-defined, reversible phase transition from the normal to the superionic state presents an opportunity to track the evolution from collective phonon excitations in the normal crystalline state to the liquid-like stochastic diffusion in the superionic regime. ~~Therefore, in this study, we examine the lattice dynamical behavior of $CuCrSe_2$ across the superionic transition.~~ The thermoelectric conversion efficiency of $CuCrSe_2$ approaches 1 at 773 K [30], due in part to a very low $\kappa_{\rm lat} \sim 1\,{\rm Wm^{-1}K^{-1}}$ [30,38–40]. Such a low $\kappa_{\rm lat}$ in a relatively light material is surprising, especially below the order-disorder temperature ($T_{\rm od}$) of 363 K. While diverse phonon scattering mechanisms have been invoked to account for the ultralow $\kappa_{\rm lat}$ in $M{\rm Cr}X_2$ [11,28,30,32,33], a detailed atomistic understanding has remained elusive, owing to the lack of ~~prior~~ phonon dispersion measurements. Here, we fully elucidate the evolution of the atomic dynamics in $CuCrSe_2$ across the superionic transition, including in single crystals, which enables us to resolve prior controversies.

We use inelastic neutron scattering (INS) and inelastic x-ray scattering (IXS) to unravel the phonon scattering processes, supplemented with transport measurements, and clarify the relation between the phonon picture of atomic vibrations and superionic diffusive behavior. Further, we compare our measurements with density functional theory (DFT) and *ab-initio* molecular dynamics (AIMD) simulations. INS measurements on powder samples enabled the accurate determination of the overall dynamics as a function of temperature, via the phonon density of states (DOS) and quasi-elastic scattering, while comprehensive momentum-resolved IXS measurements on single crystals provided a definite determination of the phonon quasiparticles through their dispersions, polarization vectors, and mode-specific linewidths. To our knowledge, these are the first detailed phonon dispersion measurements in superionic $M{\rm Cr}X_2$. Our INS and IXS experiments reveal that

propagative acoustic modes remain well-defined deep into the superionic regime amid a dramatic evolution of the Cu sublattice dynamics. Our *ab-initio* simulations fully corroborate the persistence of propagative acoustic modes in the superionic state, while the phonon quasiparticles involving predominantly the Cu-sublattice break down. Further, our results reveal the role of magnetism in stabilizing the structure, with a strong spin-lattice interaction coupling the quasi-2D hopping of Cu atoms with motions of Cr and Se atoms around them.

The crystal structure of $CuCrSe_2$ is layered rhombohedral with two possible sites for Cu atoms, α and β, as shown in Fig. 1-a,e (hexagonal representation). $CrSe_6$ octahedra 'sandwich' layers of tetrahedral α and β Cu sites. At low temperature (Fig. 1-a), Cu ions occupy only the α sites, and the structure has $R3m$ symmetry, with Cr^{3+} spins ordering antiferromagnetically below the Néel transition $T_{\mathrm{N}} = 55\ K$ [38,40,41]. Warming across $T_{\mathrm{od}} = 363\,\mathrm{K}$, an order-disorder transition occurs, redistributing Cu ions across α and β sites with equal occupancies (Fig. 1-e, Fig. S4) [31,36]. Above T_{od}, the Cu ions undergo 'superionic' quasi-2D diffusion in their half-occupied sublattice, changing the average structure to $R\bar{3}m$ [31,36].

We first track the evolution of the $CuCrSe_2$ lattice dynamics from 10 to 650 K with INS ~~measurements conducted~~ on polycrystalline samples using time of flight spectroscopy. These experiments provide the orientation-averaged dynamical structure factor, $S(Q, E)$:

$$S_{\mathrm{inc}}(Q, E) = \sum_i \sigma_i \frac{\hbar^2 Q^2}{2M_i} \exp(-2W_i) \frac{g_i(E)}{E} [n_T(E) + 1]\,, \tag{1}$$

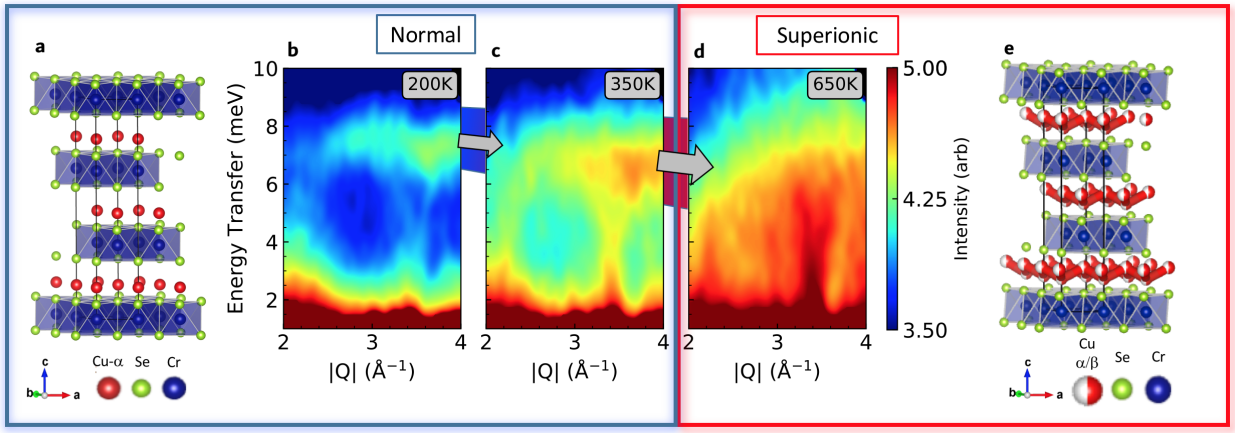

Figure 1: (color) Anomalous atomic dynamics across the superionic transition in $CuCrSe_2$. (a) Room temperature crystal structure of $CuCrSe_2$. (e) High temperature structure shown with Cu occupancy on α and β sites (indicated with half white-half red spheres). Tetrahedral hopping directions shown with thick red bands. (b-d) $S(Q, E)$ maps measured with $E_i = 15$ meV on CNCS at 200 K (b), 350 K (c), and 650 K (d). The $S(Q, E)$ maps show a dramatic softening and broadening of an intense low-energy excitation band around 8 meV, while the dispersive acoustic phonons, emanating from the 110 Bragg peak near 3.4 Å^{-1}, remain visible in the superionic phase.

where Q and E are the wavevector amplitude and energy transfer to the sample, $g_i(E)$ is the phonon DOS, σ_i, M_i, and $\exp(-2W_i)$ are the neutron scattering cross-section, mass, and Debye-Waller factor for atom i, respectively, and $n_T(E)$ is the Bose occupation factor [42] (we note $Q = |\mathbf{Q}|$ the magnitude of wave-vector transfer, E the energy). The related dynamical susceptibility is given by $\chi''(Q,E) = (1 - \exp(-E/k_{\rm B}T))S(Q,E)$.

The INS spectra reveal a dramatic temperature evolution of the atomic dynamics, as can be seen in Fig. 1. $S(Q,E)$ maps in Fig 1-(b,c,d) show a nearly flat and intense excitation band around 8 meV for $T \leq 350$ K, in addition to acoustic phonon dispersions emanating from the (110) nuclear Bragg peak at $Q = 3.4$ Å^{-1}. ~~As T_{OD} is approached,~~ Upon warming in the normal state, the modes around 8 meV show a pronounced shift to lower energy ("softening") and broadening, which becomes drastic when crossing into the superionic state, eventually spreading over most of the low energy transfer range at 650 K, while the Bragg peak and acoustic dispersions remain clearly visible (Fig. 1b-d).

The behavior of the 8 meV phonons was analyzed by integrating $S(Q,E)$ data over $3 \leq Q \leq 4$ Å^{-1}. The resulting $S(E)$ are plotted in Fig. 2-a, while Fig. 2-b shows fit results for the position and width of the peak in the corresponding $\chi''(E)$. Below $T_{\rm od}$, the phonon band strongly softens on heating and becomes constant in energy above $T_{\rm od}$. The energy decrease from 10 K to 420 K is about 20%, one order of magnitude larger than expected based on thermal expansion alone (SI), revealing a very strong anharmonicity. Most strikingly, the energy width of the low-E optical phonon band, corrected for instrumental energy resolution, broadens by a factor of four from 100 K

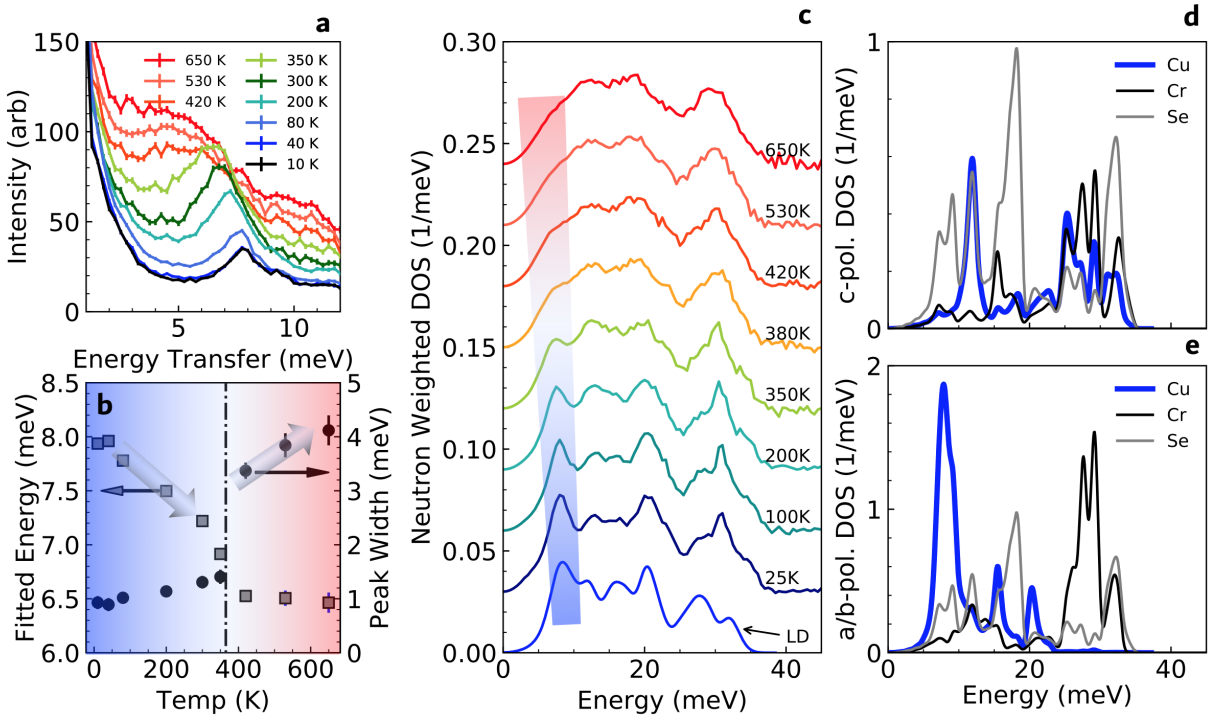

Figure 2: (color) Phonon ~~DOS~~ spectra from INS and DFT simulations, showing large damping and softening of Cu in-plane modes across $T_{\rm od}$. (a) $S(E)$ cuts, integrated over the range $3 \leq Q \leq 4\,\text{Å}^{-1}$ for all temperatures measured at CNCS. (b) Fitted energy (grey squares) and resolution-corrected peak widths (black circles) from fits to data in (a), showing the pronounced softening and extreme broadening of the 8 meV phonon-like excitation. (c) Neutron-weighted DOS from ARCS measurements at indicated temperatures. The trace labeled LD is the DOS from lattice dynamics using DFT, including neutron weighting and convolution with the instrument resolution. (d,e) Site projected DOS from DFT for the (d) c-axis polarized and (e) in-plane motions in the $a-b$ plane of the indicated atoms. Cu motions mainly contribute a strong peak near 8-10 meV for the in-plane calculation, and a weaker peak near 12 meV for c-polarizations.

to 650 K (Fig. 2-b), becoming strongly damped above $T_{\rm od}$. In the ordered phase (normal state), the width increases linearly with T, consistent with anharmonic scattering.

To determine the nature of the 8 meV mode, we analyze the DOS, $g(E)$, from both INS and DFT simulations (Fig. 2). Consistent with $S(E)$ from CNCS, the DOS shows a sharp, pronounced peak at 8 meV at low T, which undergoes a drastic broadening upon heating, and eventually disappears once the material enters the superionic phase (between 350 K and 420 K). Quite strikingly, while the low-energy peak softens significantly, the overall mean energy of the neutron-deweighted DOS (Tab. S-3) shows little change between 10 K and ~~650~~500 K, indicating a robust supporting network of $CrSe_6$ octahedra. [move this sentence to SI - it opens up an unresolved question: how can this be the case while Cu modes soften so much, since Cu modes also participate in the average?] Our DFT simulations within the quasi-harmonic approximation (QHA), including spin-polarization, yield a DOS in close agreement with INS for $T < T_{\rm od}$, as shown in Fig. 2-c. In addition, we use the DFT simulations to decompose the total DOS into the atom-resolved partial phonon DOS for atom i, defined as:

$$g_i(E) = \sum_{j,\mathbf{q}} |e_i(j,\mathbf{q}))|^2 \delta(E - E(j,\mathbf{q}))\,, \tag{2}$$

where $E(j,\mathbf{q})$ and $e(j,\mathbf{q})$ are the phonon energies and eigenvectors [2,42]. We further project the polarization components of the atom-resolved DOS onto the $a-b$ plane (Fig. 2-d) or along the c-axis (Fig. 2-e). The decomposition clearly reveals that the 8 meV peak arises overwhelmingly from in-plane modes dominated by Cu vibrations. The participation of Cu vibrations to all the different modes along the dispersions is illustrated in Fig. S18. From the temperature dependence observed in INS and AIMD simulations, as well as the reported mean square displacements [31], we

conclude that the Cu atoms already undergo large-amplitude quasi two-dimensional vibrations at low frequency ($\sim$ 8 meV) in the normal (ordered) phase, and can be considered 2D 'rattlers' by analogy with filler atoms in cage compounds and intercalation compounds [16,19,22]. The oscillations of the Cu rattlers subsequently become overdamped upon heating into the superionic phase, as Cu ions delocalize and begin to follow diffusive dynamics. ~~These changes of the Cu sublattice dynamics are reversible, as shown in Fig. S 7.~~

Determination of phonon polarizations and dispersions requires momentum-resolved measurements, and we obtained this information with IXS on small single crystals[43]. The dynamical structure factor measured using IXS is given by:

$$S(\mathbf{Q},\omega) = \left| \sum_d f_d(\mathbf{Q}) \exp(-\mathrm{W_d}) [\mathbf{Q}\cdot\mathbf{e_d}(\mathbf{q},\mathrm{j})] \mathrm{M_d^{-1/2}} \exp(\mathrm{i}\mathbf{Q}\cdot\mathbf{d}) \right|^2 \frac{\langle n\rangle + 1/2 \pm 1/2}{\omega_{\mathbf{q},j}} \delta(\omega \pm \omega_{\mathbf{q},j}) \tag{3}$$

where d is the atom index (and $\boldsymbol{d}$ the atom position) in the unit cell, $f_d(\mathbf{Q})$ is the form factor for atom d, W_d the corresponding Debye-Waller factor, $\mathbf{q}$ the phonon wave vector, $\omega_{\mathbf{q},j}$ the phonon frequency for branch index j, $\mathbf{Q}$ the wave vector transfer. Results are shown in Fig. 3. IXS spectra were collected in multiple Brillouin zones at temperatures between 300 and 600 K, across T_{od}. The phonon dispersions, $E = \hbar\omega(\mathbf{q})$, were extracted by fitting peak positions in IXS spectra using a damped harmonic oscillator profile convoluted with the instrumental energy resolution (Fig. 3-(d,e,f). The experimental dispersions are shown as markers in Fig. 3-(a,b,c), overlaid on the DFT

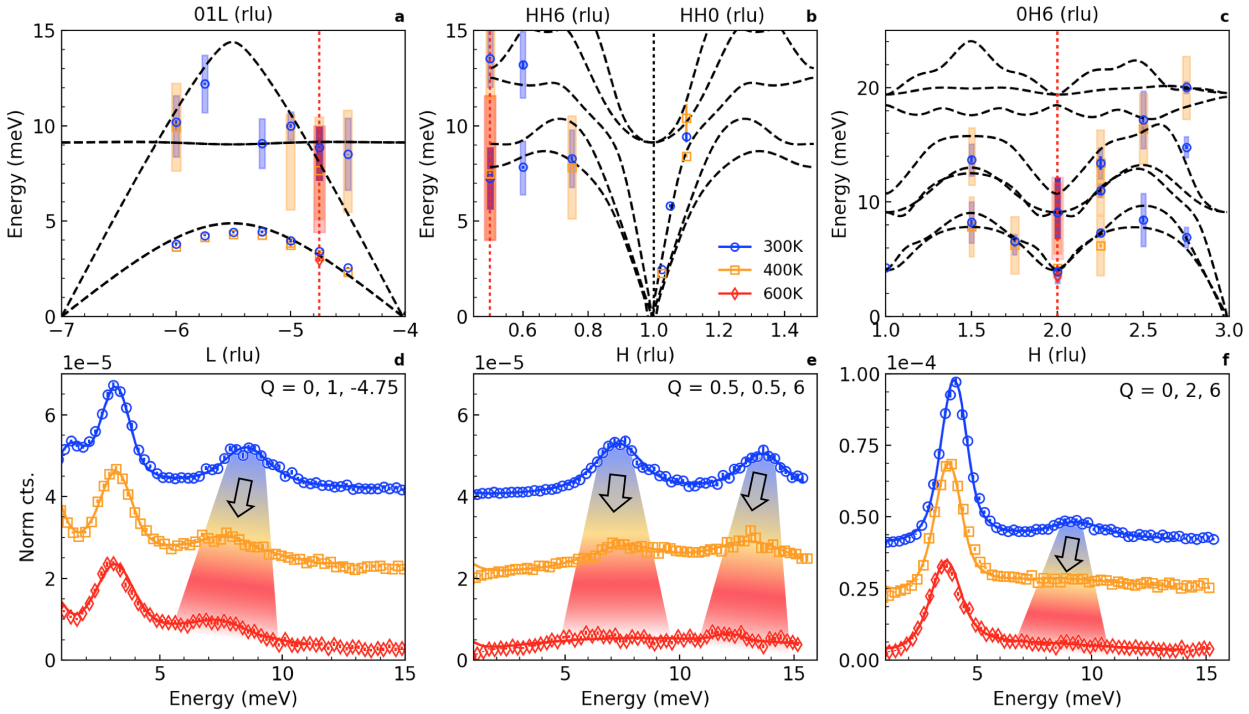

Figure 3: (color) Momentum-resolved IXS measurements on single crystalline $CuCrSe_2$, compared with DFT simulations. (a-c) Phonon dispersions measured along high symmetry directions (markers) overlaid on DFT calculations of the low temperature structure (dashed lines). Abscissa labels indicate the wave vector space direction, and red vertical dashed lines indicate the locations of constant-Q spectra in panels (d-f). Indexing is based on the hexagonal representation of the rhombohedral cell. Blue markers are data from the normal state, while yellow and red markers are measurements at 400 K and 600 K, both in the superionic state. Wide colored boxes represent extracted phonon linewidths for the indicated temperature. The spectra in (d-f) show the IXS intensities (markers) ($\chi''(E)$) and damped harmonic oscillator fits (solid curves).

simulations for the ordered phase (harmonic approximation). As one can see, the agreement between IXS data at 300 K and DFT is excellent. A low-energy, flat optical branch is observed around 8 meV, clearly seen for example along $[0, 1, L]$ (Fig. 3-a). **Calculations of anharmonically renormalized self-consistent phonon dispersions were also performed (see details in supplement).**

Comparing spectra at specific wavevectors below and above $T_{\rm od}$ allows us to track specific modes across the superionic transition. Our IXS data show that phonon modes with strong Cu character undergo strong broadening and intensity suppression across $T_{\rm od}$, effectively breaking down, in particular the phonon modes around 8 meV. Modes exhibiting strong broadening are indicated in Fig. 3-(a,b,c) with broad boxes. Both the $\sim$8 meV optic mode and the top of TA branches along [H,H,6] and [0,H,6] are dominated by Cu motions (Fig. S18). Strikingly, IXS data show very clearly that all the low-energy, propagative acoustic modes below 5 meV remain well-defined above $T_{\rm od}$ (Fig. 3 and Table S-1). These acoustic modes are the dominant contributions to the lattice thermal conductivity, as shown in our calculation of the spectral decomposition of thermal conductivity (Fig. S17). This behavior differs from reports based on INS measurements on powder samples of $AgCrSe_2$ in Ref. 32, or conclusions inferred from heat capacity in $Cu_{2-x}Se$ from Ref. 9. Although IXS measurements clearly show that dispersive acoustic modes persist in the superionic phase in all directions measured, some broadening is observed beyond the instrumental resolution, corresponding to increasing scattering of acoustic phonons above $T_{\rm od}$ (Tab. S-1) and consistent with our measurements and first-principles modeling of $\kappa_{\rm lat}$ (SFig. 21).

The extreme damping of Cu vibrational modes at 8 meV in the superionic phase, seen in all

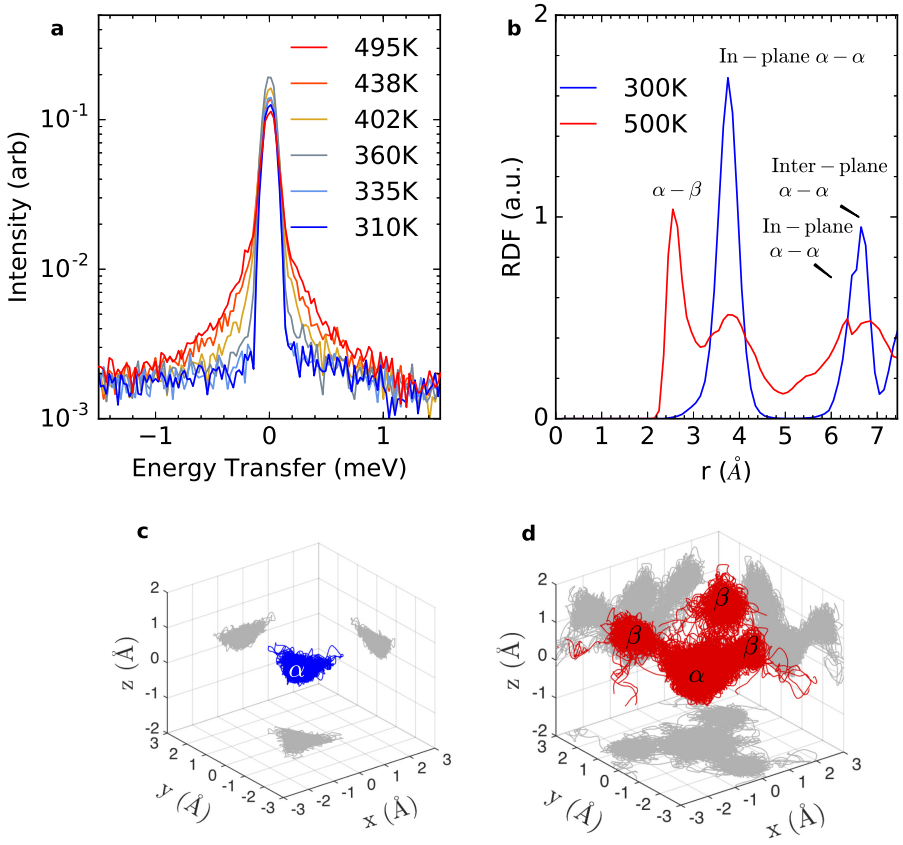

Figure 4: Diffusive behavior of Cu ions probed with quasielastic neutron scattering and *ab-initio* molecular dynamics. (a) Temperature evolution of quasielastic scattering from CNCS, for integrated over $1.4 \leq Q \leq 1.6\,\text{Å}^{-1}$. (b) Cu-Cu RDF calculated from AIMD. The peak at $r_{\alpha-\beta} = 2.6\,\text{Å}$ for T =500 K indicates random occupations of both Cu α and β sites. A considerable broadening of peaks, from large amplitude spatial fluctuations, is also seen at 500 K. (c-d) AIMD trajectories for the Cu ions from *ab-initio* molecular dynamics simulations, showing the localization of the Cu sublattice for the spin-polarized case with all atoms oscillating around α site ($z = 0$) at 300 K (c), compared to the delocalization of Cu ions across α and β ($z = 1$) sites in the non-spin-polarized case at 500 K (d).

measurements, signifies that Cu ions no longer undergo oscillatory motions. Yet, their degrees of freedom need to be preserved, and we expect that their dynamics become stochastic/diffusive instead of phonon-like. Such a behavior is expected to lead to a characteristic quasi-elastic neutron scattering (QENS) signal, which takes the form of a Lorentzian distribution as function of energy transfer, centered at the elastic line ($E = 0$) [44]. QENS results for Q = 1.5 Å^{-1} are shown in Fig. 4-a, and confirm the diffusive motions of Cu ions above T_{od}. The intensity of the Lorentzian tails strongly increases with temperature, revealing increasing Cu diffusivity ~~with~~ when $T > T_{\mathrm{od}}$. Fitting QENS data with a Q-dependent Lorentzian of full-width-at-half-maximum $2\Gamma_T(Q)$ enabled us to extract critical information about the Cu diffusivity (Fig. S 8). From the linear portion of the Γ *vs* Q^2 relation at low Q, we extracted a diffusion constant, D_T, using $\Gamma_T(Q) = \hbar D_T Q^2$ for the low Q limit [44]. We observe that $\Gamma(Q^2)$ plateaus at higher Q, characteristic of jump-diffusion in solids [44]. At $T = 495$ K, we find $D = 7.2 \pm 0.4 \times 10^{-6}$ cm^2 s^{-1}, in quantitative agreement with the diffusion constant estimated from Nernst-Einstein relation, $D = 8.9 \times 10^{-6}$ cm^2 s^{-1} at the same temperature, confirming the superionic character. The difference between these two values could arise from the quasi-2D nature of diffusion in $CuCrSe_2$, which is beyond the scope of our QENS analysis.

Above T_{od}, phonon oscillations of the lattice in the superionic phase 'see' a half filled $\alpha + \beta$ layer with 50% vacancies and a disordered distribution of Cu ions undergoing large anharmonic oscillations. The Cu disordering is evident from our neutron diffraction data (supplement Fig. 4) as well as the Cu-Cu radial distribution function (RDF) computed from AIMD (Fig. 4b). In the superionic state, a new peak appears in the RDF at about 2.5Å. This peak corresponds to nearest-

neighbor bonds $r_{\alpha-\beta}$, resulting from occupation of both α and β sites, while only $r_{\alpha-\alpha} = 3.8$ Å is seen in the ordered phase. In addition, a significant broadening is observed in RDF peaks at 500K, indicating large amplitude fluctuations in position. Thus, we understand that the copper dominated phonons in the superionic phase are strongly scattered by disorder, besides anharmonicity. These conclusions are consistent with our measurements and modeling of the lattice thermal conductivity, which is low and relatively constant above $T_{\rm od}$ (SI), in agreement with prior reports [30,40]. Using a Chudley-Elliot model[45], $\Gamma(Q) = \hbar/\tau(1 - \sin(Ql)/Ql)$ with l the jump length ($l = 2.34$ Å for α-β tetrahedral hop), we obtain an estimated mean residence time $\tau \sim 32$ ps at 382 K and still ~ 7 ps at 495 K (Fig. S 8). Thus, the time scale for diffusion hops in the superionic phase remains larger than the phonon vibrational time scale dominating thermal transport, which, from our spectral decomposition of κ_{lat}, is around 0.7 THz ($h\nu \sim 2.9$ meV) (Fig. S 17), but we emphasize that Cu ions are disordered among α and β sites at all temperatures in the superionic phase. Yet, the persistence of acoustic phonons in the superionic phase rules out the picture that κ_{lat} in a superionic compound would be necessarily reaching the minimum possible thermal conductivity [27], and is in accord with even lower values of thermal conductivity in $CuCrSe_2$ being achievable with nanostructuring [46] or alloying [28].

We now consider magnetic fluctuations seen in INS at low Q (Fig. S 5). At low T, Fig. S 5-(a,b), magnetic spin-waves are dispersing out of the antiferromagnetic Bragg peak ($E = 0$) at $Q = 2.0$ Å^{-1}. This Bragg peak disappears above $T_{\rm N} = 55$ K (Figs. S 4,5,6), as expected from the loss of long-range antiferromagnetic order. However, correlated spin fluctuations at finite E remain much above $T_{\rm N}$, and are clearly seen even above room temperature (Fig. S 5). We note

that our first-principles calculations of the DOS and dispersions captured the experimental results accurately only when including spin-polarization (collinear approximation) in DFT. Non-magnetic calculations, on the other hand, resulted in unstable phonon dispersions across the Brillouin zone (Fig. S 10), suggesting an influence of magnetic ordering on lattice stability and phonons.

In the superionic phase, the QHA used to compute phonons below T_{od} breaks down. In order to model this regime, we performed *ab-initio* molecular dynamics (AIMD) as a function of temperature (details in SI). Fig. 4-(c,d) show the resulting folded and symmetrized Cu trajectory for spin-polarized and non-magnetic AIMD simulations at 300 and 500 K, respectively. As one can see, in non-magnetic simulations at 500 K, the Cu atoms delocalize across α and β sites, while at 300 K, Cu atoms occupy the α site only. Cu migration is also observed in the non-magnetic simulations at 300 K (see Fig. S11-a), indicating that Cu delocalization is favored in absence of magnetism in AIMD. This is compatible with our QHA phonon dispersion calculations, showing that absence of magnetic correlations in DFT results in weaker bonding of Cu atoms. Experimentally, we can understand the non-magnetic behavior as more representative of the highest temperatures. At intermediate temperatures, above T_{N} but below T_{od}, short-range dynamic correlations of Cr magnetic spins persist (Figs. S5-6), and the spin-polarized calculations appear necessary to capture their influence on the lattice dynamics.

We now compare the AIMD results to the experimentally determined phonon DOS (Fig. 2c), and momentum- and energy-resolved phonon spectra (Fig. 3(d-f)) from INS and IXS measurements, respectively. From the AIMD trajectories (Fig. 4(c,d)), we computed the phonon DOS and

power spectrum (SI), taking into account anharmonicity to all orders, and including a distribution of Cu hopping times. Good agreement is found with our INS results for the phonon DOS and mean energy (Fig. S15 and Tab. S-3). The enhanced Cu hopping in non-magnetic simulations leads to a broadened Cu partial-DOS (Fig. S15), in good agreement with the experimental trend from INS. The AIMD results show a weak temperature dependence for the average phonon energy, which indicates that the dynamics of the average lattice are less sensitive to the superionic transition. The significant broadening and breakdown of Cu dominated modes [Fig. S18 and S14(c-f)] is in agreement with IXS measurements. On the other hand, despite the significant Cu hopping, we observe that low-energy propagative TA modes remain well-defined in the power spectrum (Fig. S14a) consistent with our IXS measurements (Fig. 3d). In addition, TA phonon modes near the top of the branch but having small Cu participation, as is the case at $Q = (0, 2, 6)$ and $E = 4$ meV, are also less sensitive to the superionic transition in both experiment and simulations (Fig. 3f, Fig. S14b).

From overwhelming experimental and theoretical evidence, we conclude that long-wavelength propagative TA modes remain well-defined through the superionic transition, as do phonons involving predominantly the backbone of $CrSe_6$ octahedra. Low-energy Cu-dominated modes, on the other hand, break down in the superionic state. These fundamental insights regarding atomic dynamics in an intermediate state of matter shed new light on the role of lattice dynamics in fast diffusion for the design of high-performance solid-state electrolytes, and will facilitate the emergence of superionic compounds with ultralow thermal conductivities for thermoelectric applications.

1 Methods

A powder sample of $CuCrSe_2$ was synthesized via direct solid-state reaction and the crystal structure was confirmed with x-ray diffraction and magnetization measurements. A small amount ($\sim 3\%$) of $CuCr_2Se_4$ secondary phase was detected, but this did not hinder the INS analysis (Figs. S1, S2). Single crystals for x-ray measurements were synthesized by annealing the polycrystalline precursor at 900°C for at least 2 weeks, resulting in platelet crystals 1 mm long and 30 μm thick.

The INS experiments were performed on an 8 gram powder sample of $CuCrSe_2$ with the CNCS [47] and ARCS [48] time-of-flight spectrometers at the Spallation Neutron Source at Oak Ridge National Laboratory. The ARCS measurements used an incident neutron energy $E_i = 55$ meV to probe the entire phonon spectrum over many Brillouin zones, and were used to extract the phonon DOS. Experiments at CNCS used $E_i = 15$ meV to focus on low-energy phonon modes with higher resolution, and additional measurements with $E_i = 4$ meV (elastic line resolution ~ 120 μeV) were performed to study the quasi-elastic scattering signal from diffusive behavior. Data were collected in the range from 10 K to 650 K at both instruments, using a closed cycle refrigerator. The INS data were reduced using algorithms in the Mantid analysis software [49]. The data were normalized by the accumulated incident neutron flux, and a detector efficiency correction was applied based on a normalization measurement of a vanadium standard.

QENS data from CNCS were fit with a Q-dependent Lorentzian of full-width-at-half-maximum $2\Gamma_T(Q)$, and a delta-function $\delta(E = 0)$ representing incoherent elastic scattering, both convolved with the instrument resolution (estimated as 120 μeV). From the linear portion of the Γ *vs* Q^2

relation at low Q (Fig.S 8), we extracted a diffusion constant, D_T, using $\Gamma_T(Q) = D_T Q^2$ for the low Q limit [44]. We observe that $\Gamma(Q^2)$ plateaus at higher Q, characteristic of jump-diffusion in solids [44]. At $T = 495$ K, we find $D = 7.2 \pm 0.4 \times 10^{-6}$ cm^2 s^{-1}, in quantitative agreement with the diffusion constant estimated from Nernst-Einstein relation, $D = 8.9 \times 10^{-6}$ cm^2 s^{-1} at the same temperature, thus confirming the superionic character.

Inelastic X-ray measurements were performed at the HERIX spectrometer at the Advanced Photon Source[43] on single crystals of $CuCrSe_2$ (see Fig. S9). The samples were approximately 25 μm thick. Each sample was mounted on a copper rod using commercial varnish at low temperature or silver paste at high temperature, and was measured in the transmission configuration. The incident beamline wavelength was 0.5226 Å (23.7 keV). The energy resolution of the instrument, measured with a plastic standard, was $\sim$1.50 meV in a first experiment and $\sim$1.32 meV in a second experiment. IXS spectra were collected in multiple Brillouin zones at temperatures between 300 and 600 K, across $T_{\rm od}$. A closed-cycle refrigerator with a beryllium shield was used to provide temperature control. The phonon dispersions, $E = \hbar\omega(\mathbf{q})$, were extracted by fitting peak positions in IXS spectra using a damped harmonic oscillator profile convoluted with the HERIX energy resolution.

Phonon simulations were performed in the framework of density functional theory (DFT) as implemented in the Vienna *Ab initio* Simulation Package (VASP 5.3) [50–52]. Electronic k-point meshes of $8 \times 8 \times 2$ and $12 \times 12 \times 12$ were used in the 12 atoms conventional (hexagonal) cell and the 4 atom primitive cell, respectively. The plane-wave energy cut-off was set to 500 eV. The

convergence criterion for the electronic self-consistent loop was set to 10^{-8} eV. We used projector-augmented-wave potentials, which explicitly included 12 valence electrons for Cr ($2p^6 3d^5 4s^1$), 17 for Cu ($2p^6 3d^{10} 4s^1$), and six for Se ($2s^2 2p^4$). We performed both collinear spin polarized (SP) and non-spin polarized (NSP) calculations. We used the generalized gradient approximation (GGA) in the Perdew-Burke-Ernzerhof (PBE) parametrization [53]. During the relaxation of the structure, the atomic positions were optimized until forces on all atoms were smaller than 1 meV Å^{-1} for constant experimental lattice parameters $a = b = 3.679$ Å and $c = 19.385$ Å [54]. Phonon dispersions were calculated in the harmonic approximation, using the finite displacement approach as implemented in Phonopy [55]. We used a $4 \times 4 \times 1$ supercell of the conventional cell (192 atoms), as well as a $3 \times 3 \times 3$ supercell of the primitive rhombohedral cell (108 atoms). The atomic displacement amplitude was 0.01 Å in all cases. The computed DOS was convolved with the INS spectrometer energy resolution for direct comparison with the measurement.

Ab-initio molecular dynamics (AIMD) simulations were performed on a $4 \times 4 \times 1$ supercell of the conventional cell (192 atoms). We used a Γ-point mesh with a plane-wave cut-off energy of 700 eV in all AIMD simulations. The convergence criterion for the electronic self-consistent loop was set to 10^{-4} eV. AIMD simulations were performed using an NVT-ensemble with Nosé-Hoover thermostat. The simulations were performed for about 10000 to 15000 fs for NSP, and 6000 to 10000 fs for SP, with a time step of 2 fs. Remaining AIMD parameters were kept identical to 0 K DFT phonon simulations. Lattice thermal conductivity simulations were performed using both almaBTE [56] and with phenomenological scattering models combined with the first-principles dispersions [57]. For almaBTE, a $4 \times 4 \times 1$ supercell was used to extract third-order order force

constants, which allows consideration of interaction triplets up to the third nearest neighbor. A q-mesh of $12 \times 12 \times 12$ was used.

Additional data and information about data treatment for all techniques are given in the supplementary information.

Author contributions

JLN, DB and OD performed and analyzed the neutron scattering measurements with support from GE and DLA. JLN, DB and OD performed and analyzed the x-ray measurements with support from AS. AFM synthesized the samples and performed transport measurements. TLA performed diffusivity and heat capacity measurements above 300 K. DB and JD performed simulations. JLN, DB and OD wrote the manuscript and all authors commented on the manuscript. OD supervised the project.

1. Boyce, J. B. & Huberman, B. A. Superionic conductors: Transitions, structures, dynamics. *Physics Reports* **51**, 189–265 (1979).

2. Brüesch, P. *Phonons: Theory and Experiments I*, vol. 34 of *Springer Series in Solid-State Sciences* (Springer Berlin Heidelberg, Berlin, Heidelberg, 1982).

3. Mahan, G. D. & Roth, W. L. (eds.) *Superionic Conductors* (Springer US, Boston, MA, 1976).

4. Salamon, M. B. (ed.) *Physics of Superionic Conductors* (Springer-Verlag, Heidelberg, 1979).

5. Chandra, S. *Superionic Solids*. Principles and Applications (North-Holland, 1981).

6. Kamaya, N. *et al.* A lithium superionic conductor. *Nature Materials* **10**, 682 (2011).

7. Kato, Y. *et al.* High-power all-solid-state batteries using sulfide superionic conductors. *Nature Energy* **1**, 16030 (2014).

8. He, X., Zhu, Y. & Mo, Y. Origin of fast ion diffusion in super-ionic conductors. *Nature Communications* **8**, 15893 (2017).

9. Liu, H. *et al.* Copper ion liquid-like thermoelectrics. *Nature Materials* **11**, 422–425 (2012).

10. Weldert, K. S., Zeier, W. G., Day, T. W., Panthöfer, M. & Snyder, G. J. Thermoelectric transport in Cu_7SeP_6 with high copper ionic mobility. *Journal of the American Chemical Society* **136**, 12035 (2014).

11. Damay, F. *et al.* Localised Ag+ vibrations at the origin of ultralow thermal conductivity in layered thermoelectric $AgCrSe_2$. *Scientific Reports* **6**, 23415 (2016).

12. Bailey, T. P. & Uher, C. Potential for superionic conductors in thermoelectric applications. *Current Opinion in Green and Sustainable Chemistry* **4**, 58 (2017).

13. Snyder, G. J. & Toberer, E. S. Complex thermoelectric materials. *Nature Materials* **7**, 105–114 (2008).

14. Zebarjadi, M., Esfarjani, K., Dresselhaus, M. S., Ren, Z. F. & Chen, G. Perspectives on thermoelectrics: from fundamentals to device applications. *Energy and Environmental Science* **5**, 5147–5162 (2012).

15. Nolas, G. S., Sharp, J. & Goldsmid, J. Thermoelectrics: basic principles and new materials developments. Springer (2013).

16. Keppens, V. *et al.* Localized vibrational modes in metallic solids. *Nature* **395**, 876–878 (1998).

17. Biswas, K. *et al.* High-performance bulk thermoelectrics with all-scale hierarchical architectures. *Nature* **489**, 414–418 (2012).

18. Koza, M. M. *et al.* Breakdown of phonon glass paradigm in La- and Ce-filled Fe_4Sb_{12} skutterudites. *Nature Materials* **7**, 805–810 (2008).

19. Christensen, M. *et al.* Avoided crossing of rattler modes in thermoelectric materials. *Nature Materials* **7**, 811–815 (2008).

20. Delaire, O. *et al.* Giant anharmonic phonon scattering in PbTe. *Nature Materials* **10**, 614–619 (2011).

21. Ma, J. *et al.* Glass-like phonon scattering from a spontaneous nanostructure in $AgSbTe_2$. *Nature Nanotechnology* **8**, 445–451 (2013).

22. Voneshen, D. J. *et al.* Suppression of thermal conductivity by rattling modes in thermoelectric sodium cobaltate. *Nature Materials* **12**, 1028–1032 (2013).

23. Lee, S. *et al.* Resonant bonding leads to low lattice thermal conductivity. *Nature Communications* **5**, 3525 (2014).

24. Zhao, L.-D. *et al.* Ultralow thermal conductivity and high thermoelectric figure of merit in SnSe crystals. *Nature* **508**, 373–377 (2014).

25. Li, C. W. *et al.* Orbitally driven giant phonon anharmonicity in SnSe. *Nature Physics* **11**, 1063–1069 (2015).

26. Voneshen, D. J., Walker, H. C., Refson, K. & Goff, J. P. Hopping Time Scales and the Phonon-Liquid Electron-Crystal Picture in Thermoelectric Copper Selenide. *Physical Review Letters* **118**, 145901 (2017).

27. Slack, G. CRC Handbook of Thermoelectrics. In *CRC Handbook of Thermoelectrics* (CRC Press, 1995).

28. Gascoin, F. & Maignan, A. Order–Disorder Transition in $AgCrSe_2$: a New Route to Efficient Thermoelectrics. *Chemistry of Materials* **23**, 2510–2513 (2011).

29. Danilkin, S. A. *et al.* Neutron scattering study of short-range correlations and ionic diffusion in copper selenide. *Ionics* **17**, 75–80 (2011).

30. Bhattacharya, S. *et al.* $CuCrSe_2$: a high performance phonon glass and electron crystal thermoelectric material. *Journal of Materials Chemistry A* **1**, 11289–11297 (2013).

31. Gagor, A., Gnida, D. & Pietraszko, A. Order-disorder phenomena in layered $CuCrSe_2$ crystals. *Materials Chemistry and Physics* **146**, 283–288 (2014).

32. Li, B. *et al.* Liquid-like thermal conduction in intercalated layered crystalline solids. *Nature Materials* **17**, 226 (2018).

33. Brüesch, P., Hibma, T. & Bührer, W. Dynamics of ions of the two-dimensional superionic conductor $AgCrS_2$. *Physical Review B* **27**, 5052–5061 (1983).

34. Wakamura, K., Miura, F., Kojima, A. & Kanashiro, T. Observation of anomalously increasing phonon damping constant in the β phase of the fast-ionic conductor Ag_3SI. *Physical Review B* **41**, 2758–2762 (1990).

35. Wakamura, K., Hirokawa, K. & Orita, K. Observation of characteristic phonon spectra for cage and mobile ions in the layered superionic conductor $AgCrS_2$. *Journal of Physics and Chemistry of Solids* **57**, 75–80 (1996).

36. Yakshibayev, R., Zabolotsky, V. & Almukhametov, R. Structural features and ionic transport in two-dimensional M_xYSe_2 (M = Cu, Ag; Y = Cr, Nb) mixed conductors. *Solid State Ionics* **31**, 1178 (1988).

37. Yakshibaev, R. A., Nadezhdina, A. F. & Zabolotsky, V. N. Character of Thermal Disordering of Copper Ions in $CuCrSe_2$. *Inorganic Materials* **25**, 1178–1180 (1989).

38. Tewari, G. C., Tripathi, T. S., Yamauchi, H. & Karppinen, M. Thermoelectric properties of layered antiferromagnetic $CuCrSe_2$. *Materials Chemistry and Physics* **145**, 156–161 (2014).

39. Cheng, Y. *et al.* $CuCrSe_2$ Ternary Chromium Chalcogenide: Facile Fabrication, Doping and Thermoelectric Properties. *Journal of the American Ceramic Society* **98**, 3975–3980 (2015).

40. Yan, Y. *et al.* Sintering temperature dependence of thermoelectric performance in $CuCrSe_2$ prepared via mechanical alloying. *Scripta Materialia* **127**, 127–131 (2017).

41. Engelsman, F., Wiegers, G. A. & Jellinek, F. Crystal structures and magnetic structures of some metal (I) chromium (III) sulfides and selenides. *Journal of Solid State Chemistry* **6**, 574–582 (1973).

42. Squires, G. L. *Introduction to the Theory of Thermal Neutron Scattering* (Cambridge University Press, Cambridge, 2009), 3 edn.

43. Said, A. H., Sinn, H. & Divan, R. New developments in fabrication of high-energy-resolution analyzers for inelastic X-ray spectroscopy. *Journal of Synchrotron Radiation* **18**, 492–496 (2011).

44. Hempelmann, R. *Quasielastic Neutron Scattering and Solid State Diffusion*. Oxford Series on Neutron Scattering in Condensed Matter (Oxford University Press, 2001).

45. Chudley, C. T. & Elliot, R. J. Neutron scattering from a liquid on a jump diffusion model. *Proceedings of the Physical Society* **77**, 353 (1961).

46. Bhattacharya, S. *et al.* High thermoelectric performance of $(AgCrSe_2)_{0.5}(CuCrSe_2)_{0.5}$ nanocomposites having all-scale natural hierarchical architectures. *Journal of Materials Chemistry A* **2**, 17122–17129 (2014).

47. Ehlers, G., Podlesnyak, A. A., Niedziela, J. L., Iverson, E. B. & Sokol, P. E. The new Cold Neutron Chopper Spectrometer at the Spallation Neutron Source: Design and performance. *Review of Scientific Instruments* **82**, 085108 (2011).

48. Abernathy, D. L. *et al.* Design and operation of the wide angular-range chopper spectrometer ARCS at the Spallation Neutron Source. *Review of Scientific Instruments* **83**, 015114 (2012).

49. Arnold, O. *et al.* Mantid—Data analysis and visualization package for neutron scattering and μSR experiments. *Nuclear Instruments and Methods in Physics Research Section A: Accelerators, Spectrometers, Detectors and Associated Equipment* **764**, 156–166 (2014).

50. Kresse, G. & Hafner, J. Ab initio molecular dynamics for liquid metals. *Physical Review B* **47**, 558 (1993).

51. Kresse, G. & Furthm$\ddot{u}$ller, J. Efficient iterative schemes for ab initio total-energy calculations using a plane-wave basis set. *Physical Review B* **54**, 11169 (1996).

52. Kresse, G. & Furthm$\ddot{u}$ller, J. Efficiency of ab-initio total energy calculations for metals and semiconductors using a plane-wave basis set. *Computational Materials Science* **6**, 15 (1996).

53. Perdew, J., Burke, K. & Ernzerhof, M. Generalized gradient approximation made simple. *Physical Review Letters* **77**, 3865–3868 (1996).

54. Tewari, G. C., Karppinen, M. & Rastogi, A. K. Effects of competing magnetic interactions on the electronic transport properties of $CuCrSe_2$. *Journal of Solid State Chemistry* **198**, 108–113 (2013).

55. Togo, A. & Tanaka, I. First principles phonon calculations in materials science. *Scripta Materialia* **108**, 1–5 (2015).

56. Carrete, J. *et al.* almabte: A solver of the space–time dependent boltzmann transport equation for phonons in structured materials. *Computer Physics Communications* **220**, 351–362 (2017).

57. Tritt, T. M. *Thermal conductivity: theory, properties, and applications* (Springer Science & Business Media, 2005).

Acknowledgements We thank Olle Hellman and Matthew Stone for helpful discussions. We are grateful to John Z. Tischler for algorithms enabling deconvolution of the energy resolution from the inelastic x-ray phonon scattering data. We would also like to acknowledge technical support from David Dunning, Tim Russell, and Saad Elorfi at the SNS. Neutron and x-ray scattering measurements and analysis (J.L.N., J.D., O.D.) were supported as part of the S3TEC EFRC, an Energy Frontier Research Center funded by the U.S. Department of Energy, Office of Science, Basic Energy Sciences under Award # DE-SC0001299. First-principles simulations (D.B.) were supported by the U.S. Department of Energy, Office of Science, Basic Energy Sciences, Materials Sciences and Engineering Division, under the Early Career Award No. DE-SC0016166 (PI O.D.). Sample synthesis (AFM) was supported by the U. S. Department of Energy, Office of Science, Basic Energy Sciences, Materials Sciences and Engineering Division. The research at Oak Ridge National Laboratory's Spallation Neutron Source was sponsored by the Scientific User Facilities Division, Office of Basic Energy Sciences, US DOE. This research used resources of the Advanced Photon

Source, a U.S. Department of Energy (DOE) Office of Science User Facility operated for the DOE Office of Science by Argonne National Laboratory under Contract No. DE-AC02-06CH11357. *Ab-initio* calculations were performed using resources of the National Energy Research Scientific Computing Center, A U. S. DOE Office of Science User Facility supported by the Office of Science of the U. S. Department of Energy under Contract No. DE-AC02-05CH11231. First principles simulations for this research used resources of the Oak Ridge Leadership Computing Facility at the Oak Ridge National Laboratory, which is supported by the Office of Science of the U.S. Department of Energy under Contract No. DE-AC05-00OR22725.

Competing Interests The authors declare that they have no competing financial interests.

Correspondence Correspondence and requests for materials should be addressed to J.L.N (niedzielajl@ornl.gov), D.B. (dipanshu.bansal@duke.edu) or O.D. (olivier.delaire@duke.edu).

distribute copies to the public, and perform publicly and display publicly, by or on behalf of the Government. The Department of Energy will provide public access to these results of federally sponsored research in accordance with the DOE Public Access Plan.